International Journal of Thermal Sciences 184 (2023) 107938

Contents lists available at ScienceDirect

International Journal of Thermal Sciences

journal homepage: www.elsevier.com/locate/ijts

A study on the effect of fin pitch variation on the thermal performance of a bus duct conductor

Mark Selvan [a], Mohd Sharizal Abdul Aziz [a,*], Kok Hwa Yu [a], M.S. Nurulakmal [b], H.P. Ong [c], C.Y. Khor [d]

[a] School of Mechanical Engineering, Engineering Campus, Universiti Sains Malaysia, 14300, Nibong Tebal, Seberang Perai Selatan, Penang, Malaysia
[b] School of Materials and Mineral Resources Engineering, Engineering Campus, Universiti Sains Malaysia, 14300, Nibong Tebal, Seberang Perai Selatan, Penang, Malaysia
[c] Furutec Electrical Sdn. Bhd., MK13, Plot 89, Lorong Perindustrian Bukit Minyak 11, Kawasan Perindustrian Bukit Minyak, 14100, Simpang Ampat, Penang, Malaysia
[d] Faculty of Mechanical Engineering & Technology, Universiti Malaysia Perlis (UniMAP), Perlis, Malaysia

ARTICLE INFO

Keywords:
Bus duct conductor
Heat sink
Fin pitch
Computational fluid dynamics
Heat transfer

ABSTRACT

The numerical results of this work provide an optimum design for a three-dimensional natural convection heat sink on the bus duct conductor's casing. The size of the fin pitch is regarded as a design variable. Using ANSYS FLUENT, a numerical model that closely resembles the experimental setup was created. The experimental data were compared to the IEC 60439-1 and IEC 60439-2 standards as a benchmark. Five potential fin pitch sizes (s1 = 1.0 mm, s2 = 1.5 mm, s3 = 2.0 mm, s4 = 3.0 mm, and s5 = 4.0 mm) were taken into consideration. It was shown that as the fin pitch gap size is reduced, the average surface temperature falls. According to the investigation, conduction resistance increased while convective resistance reduced as the fin pitch gap size grew. The overall heat resistance did, however, rise. The optimal fin pitch size, s1 = 1 mm, outperformed the other fin pitches in terms of thermal performance. The current numerical analysis expects an improved knowledge of the influence of fin pitch on a bus duct conductor's thermal performance.

1. Introduction

Many engineering systems use natural-convection heat sinks as cooling units because they are affordable, dependable, and efficient. These systems typically generate a lot of heat, thus operating at high temperatures. One such system is the electrical bus bar conductor, which aids the distribution of electrical power in large facilities. The cross-sectional shapes of these conductors range from rectangular to round. These conductors mostly link different components, such as generators, transmission lines, and loads. Bus bar conductors have a number of benefits over conventional conductors, including relatively affordable installation and maintenance compared to other electrical distribution systems.

As in any other electrical conductor, the capacity to carry current is greatly influenced by the temperature of the conductor itself. The temperature rise can be attributed to the electrical energy loss in Joule heating or Ohmic heating. The more heat is dissipated as the current flow increases, and the hotter things get until a thermal limit is reached, imposing a maximum current carrying capacity constraint. Thus, it is imperative to gauge the thermal performance of the system by measuring the average temperature of each component constituting the system.

The International Standard IEC 61439-6 lays out a detailed guideline to gauge the thermal performance of the bus duct housing. These include many expensive laboratory tests. To save cost on product development, a robust and adequate theoretical design would be needed. This situation would allow exploring several different designs at a relatively low cost. Several factors contribute to the thermal performance of the bus bar conductor, such as the amperage, cross-sectional dimensions, layout, and thermal conductivity [1]. Bus bar conductors typically comprise an aluminum housing, whereas the conductors are copper alloys. To improve the thermal performance of the bus bar conductor, optimizing the design of the heat sink of the housing is the aim of the research.

Natural convection heat sinks are one of the most ingenious forms of thermal management in technology, machinery, and even natural systems. These components are so common in everyday applications that they are sometimes easy to overlook. Heat sinks are extended surfaces that increase the heat flow away from a particular device of interest. It

* Corresponding author.
E-mail address: msharizal@usm.my (M.S. Abdul Aziz).

https://doi.org/10.1016/j.ijthermalsci.2022.107938
Received 12 April 2022; Received in revised form 16 August 2022; Accepted 12 September 2022
Available online 26 September 2022

accomplishes this task by dividing a volume into smaller sections to increase the surface area exposed to the fluid around it.

There are three distinct heat sink configurations which are active, passive and hybrid. Passive heat sinks rely on natural convection, active on forced air, whereas hybrid is a mix of both worlds. This research focuses primarily on the design and optimization of passive heatsinks. Research on improving the performance of heat sinks is abundant. An experimental analysis on the performance of various microprocessor heat sinks operating in a free stream was carried out by M.A.Ismail et al. [2]. It was determined that increased surface area and ideal fin density produced more excellent heat sink performance. When Cheng-Hung and Wei-Yu [3] looked at an improved design for a three-dimensional natural convection heat sink, they found that fin shift displacement rather than fin height played a crucial role in enhancing the heat sink's thermal efficiency. Perforations in the fin base exposed to natural convection enhanced ventilation and heat transfer performance by a factor of 2.0–2.7, according to Guei-Jang Huang et al. [4]. On the other hand, Mehran ahmadi et al. [5] investigated the thermal performance of rectangular interrupted fins exposed to natural convection. Their research showed that vertically mounted rectangular fins can considerably enhance thermal performance and that an optimum fin interruption exists.

Most heat sink performance research is primarily concerned with geometrical changes. One such research is by Ozgur Ozdilli [5], who discovered that introducing radial and axial thin channels expanded the model's surface area by 24% and enhanced its thermal performance by about 5%. Hong-Long Chen et al. [6] compared the rectangular and trapezoidal fin performance and found an insignificant performance difference. Dhamyaa S.Khudhur et al. [7] performed almost similar research on differently shaped fins. They showed that straight fins with added semicircular had a 38% increase in heat transfer coefficient compared with other fins. Geometric alterations enhance the heat sink's thermal efficiency while reducing the overall weight, volume, and price of heat sink integration. Some other common geometrical modifications that are proven to improve the thermal performance of fins are interruptions, slots, and perforations [8]. Besides, the presence of a wavy surface influenced the properties of the flow field under natural convection [9]. The increase in amplitude–wavelength ratio resulted in higher velocity fluctuation, temperature, and concentration field of the wavy surface. The buoyancy ratio crucially affects the vertical wavy surface's heat and mass transfer rate. Thus, the wavy surface can be considered in the heat sink design to enhance the heat sink performance.

C.J.Kobus and T.Oshio [10] carried out a detailed study to investigate the thermal performance of a pin-fin heat sink and, at the same time, developed a robust theoretical model that was capable of predicting the thermal performance of various geometrical patterns of a heat sink. They concluded that the convective heat transfer coefficient increased as the pin diameter decreased. It was also found that increasing the pitch size decreased the fin bundle effect near the natural convection domain, increasing the convective heat transfer coefficient.

Liu, Huang, and Wang [11] carried out theoretical and numerical studies for heat exchangers. They concluded that several design parameters enhance fin effectiveness. For example, the fin's material choice reduces the fin thickness ratio to channel radius and operates under a low convective coefficient environment. Besides, fin efficiency was improved similarly by choosing materials of high thermal conductivity, thick fin, and low convective coefficient of the fluid. Basim and Ammar [12] investigated a new plate-fin heat sink design with a fillet profile. The numerical model showed superior performance for both corrugated half-round pins and symmetrical half-round pins subjected to parallel and impinging flow.

In recent years, the rapid growth of energy consumption has demanded more advanced, high-performing thermal heat sinks exposed to natural convection. Exotic designs of all kinds of heat sinks were investigated. Su Min and An Liang's [13] focused on one exciting fractal design. They found out that the presence of a fractal grid had a significant influence on the thermal performance of the plat-fin heat sink. An impressive 43%–57% increase in convective heat transfer was achieved. Moreover, Chi-Chuan and Kuan-Yu [7] also studied the application of semi-dimple vortex generators on fin heat exchangers. Their study revealed that a larger fin pitch of 2 mm improved the thermal performance by 10% more than the plain fin geometry but at the same time resulted in a higher friction factor.

Various nanoparticles have been experimented with to enhance the heat transfer performance of the microchannel heat sink. Mehdi and Saeed [14] assessed the thermal performance of a micro-channel heatsink using a hybrid nanofluid containing graphene-silver. In their assessment, several notable findings were made. An increase in either velocity or nanoparticle concentration reduced the surface temperature for both heat sinks. A more excellent cooling uniformity was also achieved by the same means. Almost similar research was also carried out by C.J.Ho et al. [15].

The overall weight is essential in the bus duct's heat sink design. Several studies were carried out to investigate several geometries on its thermal performance and overall weight. Young Jin and Sung Jin conducted this kind of study. They suggested that varying the fin density is very useful for enhancing the thermal performance and decreasing the overall weight of the heat sink attachment cooled by natural convection [16]. One major challenge in electronic equipment is that they generate high heat flux but with a relatively low exposed surface area to natural convection. Xiaoming Huab and Chunyu Shin developed a novel fin array of unequal and continuously changing heights to address this problem. This design was aimed at improving thermal performance by reducing flow resistance. They learned that fin arrays with more significant differences in height developed lower flow resistances and created higher local heat transfer coefficient regions [17].

In any natural convection process, the orientation of the exposed surface area plays an integral role in thermal performance. According to IEC 60439-1 and IEC 60439-2, the bus bar trunking run shall be supported horizontally at approximately 1 m from the floor. Nico and Kyoung [17] investigated the effects of orientation on hybrid fin heat sinks (HFHSs) using computational and experimental methods. Their investigation showed that the lowest thermal resistance was obtained at an orientation of 45°. Similar studies were also conducted on the effects of orientation on natural convection by IIker Tari and Mehdi [18], E. Sparrow [19], and D.Jang [20].

Non-segregated bus bars are typically housed in a single housing with no barriers between phases. The only electrical insulation layer is commonly a thin polyester insulator material. The choice of insulation material is critical to the safety and performance of the bus bar conductor. Xiongyi and Yuntao [21] conducted experiments to study the most suitable insulation method for a bus bar conductor. The wet-winding process, which employs a vacuum compaction step, was proposed to be the most suitable.

Several studies were conducted in order to develop thermal models of conductors exposed to natural convection conditions. These models are essential in pursuing performance enhancement and design improvements of conductors. Zhang and Ying [22] proposed a thermal model to calculate the axial temperature distribution of overhead conductors under particular controlled conditions. Similar studies were also conducted by Xiaoming [23]. In the study, an accurate analytical model was developed to consistently produce more precise and reliable models of transmission line conductors. Mateusz et al. [24] presented an advanced model that couples both thermal and electromagnetic fields using 2-way system coupling. The results obtained a high degree of agreement against the experimental measurements in that study. Yogesh K.Prajapati [25] and Prabhakar Bhandari [26] both performed an intensive investigation to study the effect of varying fin heights in heat sinks exposed to natural convection. Heat transfer and fluid flow behavior were closely analyzed to understand the thermal performance of the heat sinks. It was deduced that as the height of the fin increases, the heat transferred to the surroundings increases as well. However, as

predicted, shorter fins did not display optimal thermal performance. Wadhah H. Aldoori [27] arrived at almost similar conclusions with the study on the effect of fin height on forced convection heat transfer from a rectangular fin array. Her study suggested that the temperature difference between the block's surface and the flowing air increases with increasing Reynolds number.

Bejan [28] first suggested constructal theory in 1996. The fundamental idea behind this theory is that in systems with finite-size flows, the structure of the system adapts to make the internal "flow" flow more easily. The constructal theory has been used to understand and construct a variety of structures, particularly when it comes to heat transfer applications. One such example was done by Huijun Feng et al. [29], who carried out a structural design of a tree-shaped compound heat transfer channel for a disc heat generation body using this theory. Both thermal and fluid flow performances were seen to increase after employing constructal design. Almost similar research was also conducted by Kun Sun et al. [30] and Zhiming et al. [31]. The constructal theory has been widely applied in various fields, from the optimization of marine condensers to the design of boiler superheaters. Several notable studies were carried Huijun Feng et al. [32–37] to improve the heat transfer and the fluid flow performance for various heat transfer applications using this theory.

Thermal fins have a wide range of engineering applications, from car radiators to heat exchangers in power plants. Ebrahim Rahmani [38] conducted a study on solar air heaters and found that increasing the fin height significantly increased thermal performance. Besides, Ahmet Ali Sertkaya et al. [39] reported that thermal performance enhancement mechanisms are chiefly due to increased heat transfer surface area. The thermal performance could be theoretically achieved by decreasing the fin pitch or increasing the fin length. Yue-Tzu Yang and Huan-Sen Peng [40] conducted a numerical study of the pin-fin heat sink with non-uniform fin height. Their research indicated that increasing the fin height near the center of the heat sink reduces the junction temperature. The effects of varying the fin height and the fin density in pyramidal pin fins were investigated by Yannick Cormier et al. [41]. Increasing these parameters increased the total thermal conductance while increasing the pressure loss across the heat sink.

In order to ensure peak performance of the bus duct conductor, the bus duct's housing has to avoid a temperature rise of more than 55 °C. An increase in temperature would reduce the current carrying capacity of the conductor. However, investigation on the effect of fin pitch of the bus duct's housing is limited. Thus, this study investigates and determines the optimal size for the best thermal performance. An accurate numerical model is developed and validated using the experimental temperature readings carried out according to IEC 60439-1/2. In the current research, ANSYS 2021 was the software of choice to perform this task. ANSYS was used to model the thermal equations to study the effect of fin pitch variation on the bus duct conductor's thermal performance. A better understanding of the effects of geometry variations will facilitate the design of a better thermal-performing bus duct conductor casing.

2. Mathematical equations

The governing equations are the most fundamental mathematical equations in any CFD code, such as ANSYS FLUENT. They represent mathematical statements of the conservation laws of physics. The convective heat transfer characteristics of the fluid domain around the bus duct conductor are achieved by solving these governing equations. The Navier-Stokes equation, continuity, momentum, and energy equations are described below. Equation (1) describes the mass conservation equation. The mass conservation equation states that matter may neither be created nor destroyed. The rate of change of mass within a control volume is always the same as the mass flux crossing the surface of the volume [42],

$$\rho\left(\frac{\partial u}{\partial x}+\frac{\partial v}{\partial y}+\frac{\partial w}{\partial z}\right)=0 \tag{1}$$

where fluid velocity V at any point is described by the local velocity components u, v, and w, which are functions of the location of the point as described by (x,y,z) and time (t).

$$\frac{\partial u}{\partial t}+u\frac{\partial u}{\partial x}+v\frac{\partial u}{\partial y}+w\frac{\partial u}{\partial z}=-\frac{1}{\rho}\frac{\partial \rho}{\partial x}+v\frac{\partial^2 u}{\partial x^2}+v\frac{\partial^2 u}{\partial y^2}+v\frac{\partial^2 u}{\partial z^2} \tag{2}$$

$$\frac{\partial v}{\partial t}+u\frac{\partial v}{\partial x}+v\frac{\partial v}{\partial y}+w\frac{\partial v}{\partial z}=-\frac{1}{\rho}\frac{\partial \rho}{\partial x}+v\frac{\partial^2 v}{\partial x^2}+v\frac{\partial^2 v}{\partial y^2}+v\frac{\partial^2 v}{\partial z^2} \tag{3}$$

$$\frac{\partial w}{\partial t}+u\frac{\partial w}{\partial x}+v\frac{\partial w}{\partial y}+w\frac{\partial w}{\partial z}=-\frac{1}{\rho}\frac{\partial \rho}{\partial x}+v\frac{\partial^2 w}{\partial x^2}+v\frac{\partial^2 w}{\partial y^2}+v\frac{\partial^2 w}{\partial z^2} \tag{4}$$

Equations (2)–(4) describe the conservation of momentum in the fluid, known as the Navier-Stokes equations, where v is the kinematic viscosity, and ρ is the fluid density [43,44].

Newton's law of cooling describes the heat transfer rate from a surface at a specific temperature T_s to the surrounding medium at T_∞, as shown in Equation (5).

$$\dot{Q}_{conv}=hA_s\,(T_s-T_\infty) \tag{5}$$

where,

A_s = Heat transfer surface area
h = convection heat transfer coefficient

The fin equation is derived by considering a volume element of the extended surface (fin) at a given location x having a length of Δ. Under steady-state conditions, the energy balance is expressed as the following:

$$\dot{Q}_{cond,x}=\dot{Q}_{cond,x}+\Delta x+\dot{Q}_{conv} \tag{6}$$

where,

$$\dot{Q}_{conv}=h(p\,\Delta x)(T-T_\infty) \tag{7}$$

Substituting and dividing by Δx and taking the limit of Δx as it approaches 0 gives,

$$\frac{\partial \dot{Q}_{cond}}{\partial x}+hp(T_s-T_\infty)=0 \tag{8}$$

Substitution of Fourier's law of heat conduction into Equation (8) results in the differential equation governing heat transfer in fins as described in Equation (9).

$$\frac{\partial}{\partial x}\left(kAC\frac{\partial T}{\partial x}\right)-hp(T_s-T_\infty)=0 \tag{9}$$

The conservation of energy derives from the first law of thermodynamics. It states that the time rate of energy change is equivalent to the net rate of heat added plus the net rate of work done in a system. The conservation of energy equation is described in Equation (10). The first term describes the local acceleration, and the second, third and fourth terms describe the advection. The fifth, sixth, and seventh terms describe the temperature flow due to heat conduction, where k is the specific heat capacity, and Cp is the specific heat capacity.

$$\frac{\partial T}{\partial t}+u\frac{\partial T}{\partial x}+v\frac{\partial T}{\partial y}+w\frac{\partial T}{\partial z}=-\frac{k}{\rho C_p}\frac{\partial^2 T}{\partial x^2}+\frac{k}{\rho C_p}\frac{\partial^2 T}{\partial y^2}+\frac{k}{\rho C_p}\frac{\partial^2 T}{\partial z^2} \tag{10}$$

3. Computational approach

3.1. Geometrical model

The commercial CFD code ANSYS FLUENT 2021R was used to

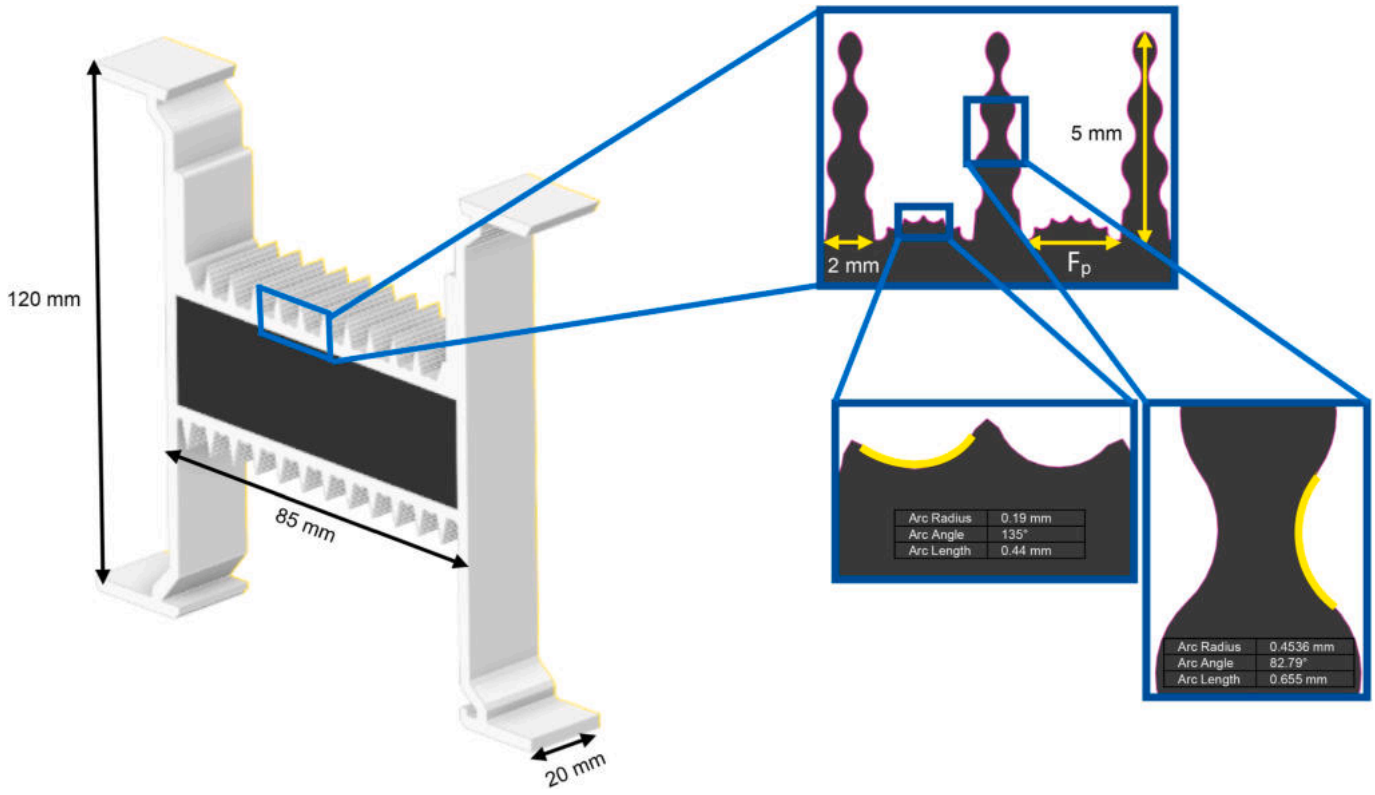

Fig. 1. Dimension and geometrical setup.

complete the numerical simulation of the bus duct conductor used in this investigation. Pre-processing, fluent setup and post-processing are the three phases of the simulation. The design of the bus duct conductor and the geometry meshing make up most of the pre-processing stage's operations. AnSYS Spaceclaim was used to create the geometry, which was then imported into FLUENT for meshing. The meshed geometry was exported to the FLUENT solution for the simulation setup when the pre-processing phase was completed. The exact dimensions of the AH Copper Bus Duct utilized in the experimental setup were used to design the model. The bus duct's measurements and geometry are shown in Fig. 1.

3.2. Mesh setup

The geometry was meshed using Fluent meshing (Fig. 2). Poly-hexcore combines disparate meshes with polyhedral elements. The minimum surface mesh size was set to 0.0001473 with a growth rate of 1.2 while enabling the curvature and proximity size functions. The fluid domain was augmented with boundary layers. Three boundary layers with a transition ratio of 0.272 and a growth rate of 1.2 were included. Poly-hexcore cells with a minimum and maximum cell length of 0.0001473 and 0.0047136 were used to fill the volume mesh. The total number of elements was approximately 1.4 million. The grid independence test determined the optimal number of elements, as discussed in the following section.

3.3. Grid independence test

In any simulation study, the grid independence test must be conducted. This test guarantees that grid elements have no impact on the simulation's outcome. While a fine mesh requires more computer power, a coarse grid may not yield accurate results. The grid independence test was run to determine the best compromise between the two. Additionally, because it reflects the main finding of the numerical analysis, the total heat transfer rate was selected as the parameter to compare the independence results. The grid independence test result is summarised in Table 1. Different mesh sizes were created from the coarse to the fine grid. It correspondingly was labeled Mesh A, Mesh B, Mesh C, Mesh D, and Mesh E, with an element size of 9.05×10^5, 1.04×10^6, 1.65×10^6, 2.61×10^6, and 3.64×10^6, respectively. The discretization error was determined from the difference of each case compared to case number 5 (Mesh E). It was observed that Mesh D had the lowest discretization error of only 0.22%. The total heat transfer rate steadily increased until Mesh D. It continued to have a steady reading as the number of elements increased. This situation indicated that the error resulting from discretization error was reduced to an acceptable level, and grid independence was reached. Therefore, Mesh D was the most optimal mesh choice for a reasonable computing time and accurate results for the current study.

3.4. Boundary and initial conditions

Fig. 3 illustrates the boundary conditions and the cell zones of the simulation setup. The setup comprises three cell zones: the fluid domain, heat sink, and the conductor. The heat sink's material is aluminum, thus having a thermal conductivity of 202.4 W/mK and an internal emissivity coefficient of 0.09. The thermal conductivity for the copper conductor was set at 387.6 W/mK and an internal emissivity coefficient of 0.05. The outlets were set as 0 Pa of gauge pressure to simulate natural convection and ensure no elements of forced convection were introduced into the simulation domain. Wrapped around the copper conductor is a thin polyester electric insulation material with a thickness of approximately 0.000125 mm, a thermal conductivity of 0.14 W/mK, and specific heat of 1.34 kJ/kg. The fluid domain was set to air using default ANSYS FLUENT's settings. The operating temperature was set to 30 °C, operating pressure was set to 101325 Pa, and operating density was set to 1.225 kg/m^3.

The heat source was a crucial piece of the puzzle in the simulation setup. The heat loss in the form of Joule losses for one volumetric heat

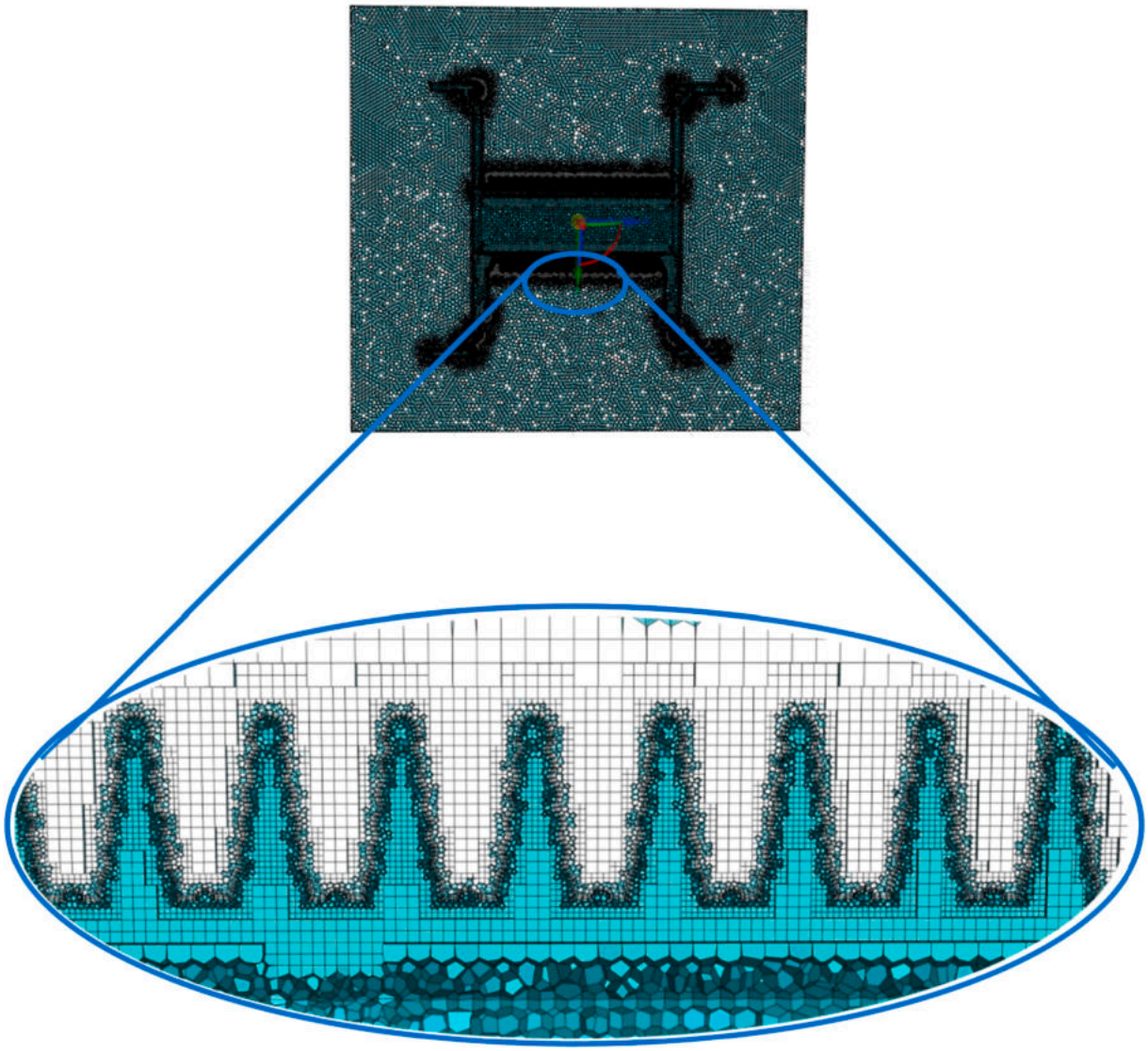

Fig. 2. Mesh grid and three boundary layers details around the heat sink.

Table 1
Mesh independence test results.

Mesh	A	B	C	D	E
No of elements	905326	1035493	1653854	2614614	3641221
Skewness	0.853	0.838	0.800	0.806	0.800
Total heat transfer rate (W)	3.445	3.461	3.485	3.486	3.478
Deviation from case 5 (%)	0.95	0.47	0.22	0.22	0.00
Computing Time (h)	7.0	8.1	9.5	10.3	13.4

source was considered. As both heat and electricity were involved, the Thermal-electric analysis system was employed to study the magnitude of the heat source. Equations (11) and (12) are used to calculate Joule losses from the bus bar using the analytical method.

$$P_{joule} = I^2 R \tag{11}$$

$$Q = \frac{P_{joule}}{V} \tag{12}$$

$$\mathrm{R} = \rho \times \frac{L}{S} \tag{13}$$

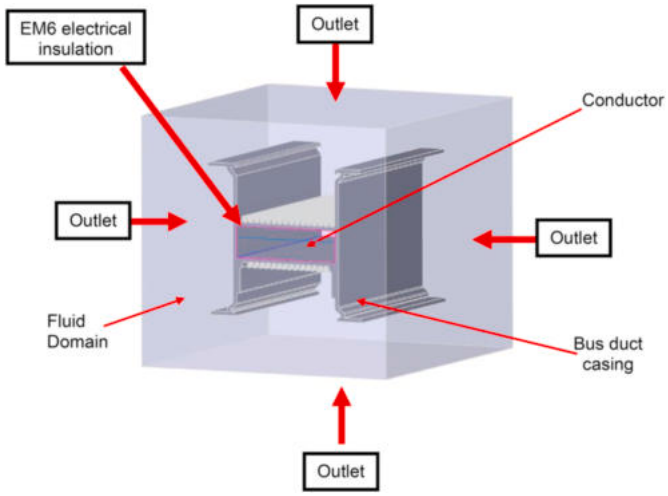

Fig. 3. Boundary conditions.

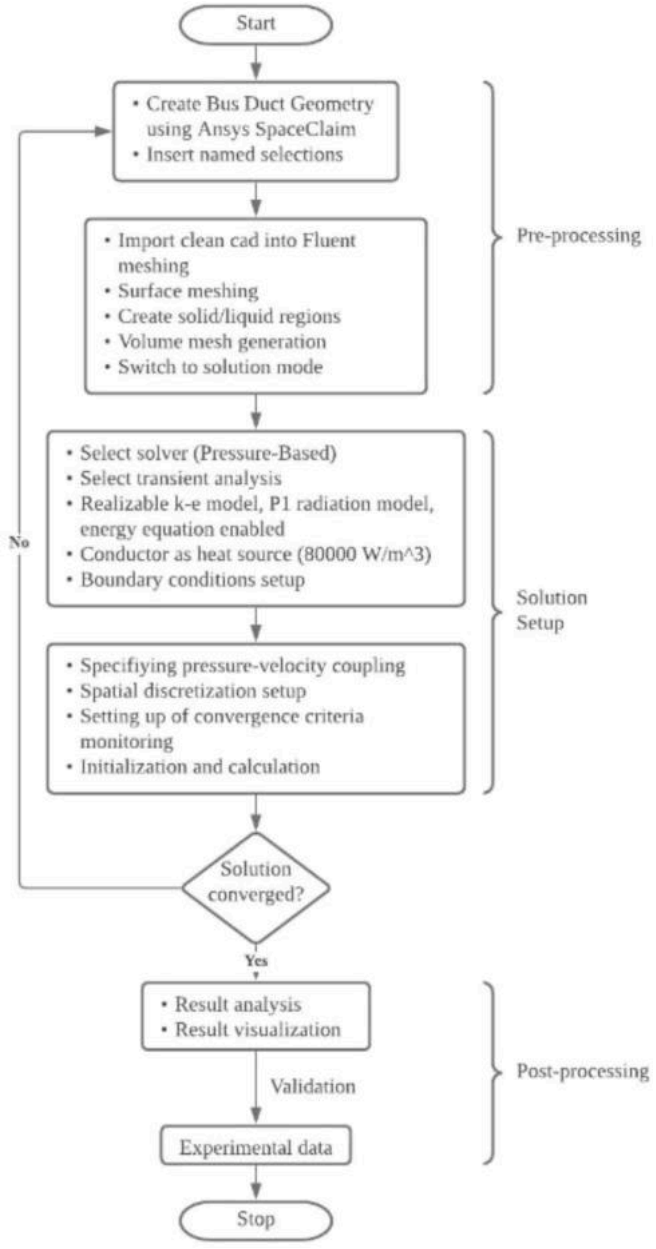

Fig. 4. Simulation setup flowchart.

where,

Q = heat loss (W/m^3)
V = Volume of geometry (m^3)
P resistivity (kg·m^3·s^{-3}·A^{-2})
L = length (m)
S = Cross-sectional area (m^2)

The current was set at 1500 A. Equation (11) states that the Joules losses are the product of the squared of the current multiplied by the electrical resistance for the length of the conductor. A simplified analytical calculation that ignored skin and proximity effects and assumed a direct current flowing through the conductor yielded a Joule loss of 86440.68 W/m^3. A similar numerical calculation was conducted using the ANSYS Thermal-Electric system yielded a Joule loss of around 90000 W/m^3, thus a deviation of 3.95%.

Table 2
Model constants.

Constant	value
$C_{1\epsilon}$	1.44
$C_{2\epsilon}$	1.92
C_{μ}	0.09
σ_k	1.0
σ_ϵ	1.3

3.5. Simulation setup

The three primary governing equations in the FLUENT CFD code are the 3-D mass conservation (continuity), momentum and energy equations. These equations solve the flow and temperature fields in the simulation. The transient approach is used as the temperature differences in the simulation domain are relatively big. This is due to the fact that in modeling natural convection, the solution highly depends on the mass inside the simulation domain. Thus, this mass will not be known unless the density is included prior to the simulation. In the transient approach, the initial pressure and temperature are used to compute the initial density. The pressure-based solver and realizable k-e model are used to predict the spreading rate of both planar and round jets more accurately. This model also has a higher probability of providing superior performance for flows involving rotation, boundary layer under strong pressure gradients, separation, and recirculation. The P1 radiation model was included in the simulation setup. It requires lower computational resources and works well with sizeable optical thickness applications. The fluid domain and the heat sink participate in the radiation heat transfer.

PRESTO! was employed as the spatial discretization method for the pressure-based solver. PRESTO! is typically chosen for natural convection and buoyancy-driven flows as well as flows with a high Rayleigh number of natural convection. In order to improve the accuracy of the results, the second-order upwind discrimination scheme was chosen to achieve higher-order accuracy at the cell faces. This scheme is done by using the Taylor series expansion about the element's cell centroid. Gravitational acceleration was enabled in the positive-X direction with a value of 9.81 m/s^2. The simulation was initialized using the standard method with the initial temperature set to 30 °C. In order to simulate the heat transfer until steady-state with no fluctuations in temperature on the heat sink, a time step size of 0.01s and 200000-time steps were chosen. Fig. 4 depicts the overview of the flow chart of the simulation setup used in the current study.

3.6. Standard k - Є model

The standard k- Є model is widely used in the application of flow numerical calculation due to its reasonable calculation accuracy, broad application range, and low computing cost [45]. The transport equations for the model were derived using experimental data. The turbulence kinetic energy (k) and turbulence dissipation rate (Є) are used in the conventional k - Є model.

The k-epsilon model has derived under the premise that the flow is entirely turbulent and that molecular viscosity has little impact.

$$\frac{\partial}{\partial t}(\rho \mathrm{k}) + \frac{\partial}{\partial \boldsymbol{x_i}}(\rho \mathrm{k} u_i) = \frac{\partial}{\partial x_j}\left[\left(\mu + \frac{\mu_t}{\sigma_k}\right)\frac{\partial k}{\partial x_j}\right] + G_k + G_b - \rho \epsilon + S_k + Y_M \quad (14)$$

$$\frac{\partial}{\partial t}(\rho \epsilon) + \frac{\partial}{\partial \boldsymbol{x_i}}(\rho \epsilon u_i) = \frac{\partial}{\partial x_j}\left[\left(\mu + \frac{\mu_t}{\sigma \epsilon}\right)\frac{\partial \epsilon}{\partial x_j}\right] + C_{1\epsilon}\frac{\epsilon}{k}(G_k + C_{3\epsilon}G_b) - C_{2\epsilon}\frac{\epsilon^2}{k}\rho + S_\epsilon \quad (15)$$

The model constants are shown in Table 2.

These default values for fundamental turbulent shear flows, such as homogenous shear flows and decaying isotropic grid turbulence, have

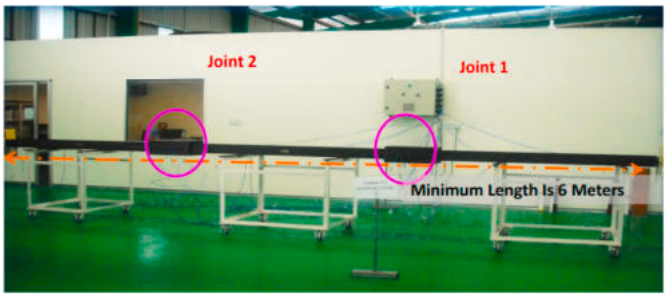

Fig. 5. 6 m long bus bar units.

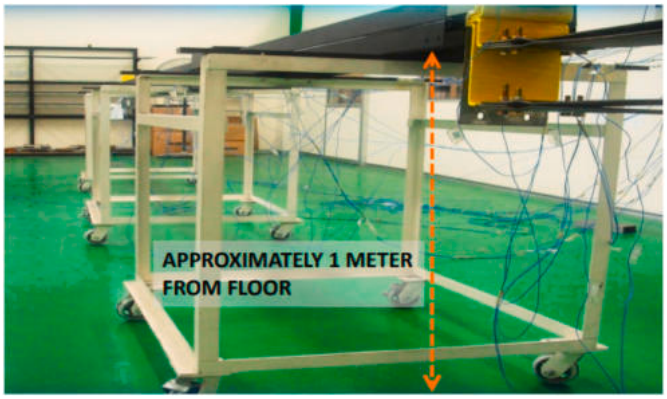

Fig. 6. Supported 1 m away from the floor.

been established through tests with air and water. For a variety of wall-bounded and free shear flows, they have been found to function reasonably effectively.

4. Experimental setup

The International Standard IEC 61439-6 [1] was used to evaluate the busbar trunking system's (BTS) performance. This standard is commonly employed in the industry to establish many electrical, mechanical, and fire-safety requirements.

Fig. 5 shows two bus bar units that have been linked together to form a total length of 6 m, including the length of the two joints. In accordance with sub-clause 10.10.2.3.5 of the IEC 61439-1 standard, the bus bar trunking was supported at approximately 1 m from the floor for horizontal orientation, as shown in Fig. 6. The test was carried out at the local ambient temperature of the test room. The local ambient temperature was part of the test report and was recorded in the immediate vicinity of the center of the bus bar trunking run under test, at the same level and a distance of approximately 1 m from one of the longitudinal sides of the enclosure for horizontal orientation (Fig. 7a). The test room did not have forced airflow as well.

The incoming terminals of the bus bar trunking feeder units were connected to a low voltage supply 50 Hz frequency, and the other end of the conductors was short-circuited (Fig. 7b). The test was conducted for a sufficient time for the temperature rise to reach a constant value (not exceeding 8 h). In practice, this condition is reached when the variation does not exceed 1 K/h. Temperature rises of the conductors and corresponding parts of the enclosure were recorded with thermocouples located in the center of each bus bar trunking unit and the adjacent joints. In Table 3, each component's allowed temperature rise as defined by IEC 61439-1 is listed.

5. Experimental validation

5.1. Experimental data

The simulation setup must be validated against experimental data to provide confidence in the simulation's accuracy and robustness in any numerical investigation. Validation typically involves conducting experiments in a laboratory environment as specified by specific relevant standards associated with the application of interest. The boundary conditions in the numerical model must as closely as possible comply with settings in the experimental setup (Fig. 7a and b). Minimal differences between the performance indicators in both the numerical and experimental setup are strongly desired, on average in the range of below 10% error. In this study, the primary performance indicator is the average surface temperature of the casing, which was measured using the K-type thermocouples. Fig. 8 presents the temperature rise for each component of the bus duct conductor. The maximum temperature rise recorded at the casing was 84.8 °C.

5.2. Comparison between experimental and simulation temperature results

The temperature of the casing from the numerical solution reached a steady-state temperature of 81.3 °C after 2000 s (33.33 min). This shows that the experimental and the simulation data's deviation was relatively minimal, with a percentage difference of only 4.12%. This result indicated that the current simulation is reliable for predicting the bus duct conductor's thermal characteristics and suitable for extending the study on the fin pitch effect. From the simulation model, the total heat transfer rate from the heat sink's surface was 1.82 W, with a net surface heat transfer convective coefficient of 3.604 W/m^2 K.

6. Fin effectiveness and fin efficiency

6.1. Fin effectiveness & efficiency

Fin effectiveness is simply the ratio of the actual heat transfer rate from a fin to the heat transfer rate without a fin, as described by equation (6). Effectiveness informs the engineer if the addition of fins helps increase heat transfer from a surface compared to a surface without any fins attached. On the other hand, fin efficiency measures how well a thermal fin performs, as described by equations (16)-(17). It is a dimensionless parameter formulated by the ratio of actual heat transfer of the fin to its ideal heat transfer if the entire fin were at the same temperature. The assumption needed to calculate the maximum heat transfer rate is that the temperature of the entire fin surface is maintained at a constant rate as the base temperature. Fin effectiveness can be enhanced in the following ways by preferably using high thermal conductivity and low-density material. Thus, aluminum is commonly employed in the design of thermal fins. The P/A ratio should also be high, meaning thin fins offer superior thermal performance, reducing the convective heat coefficient. This means thermal fins are more effective in gas than liquid. Fin effectiveness should be greater than 1 to justify fins on the surface as thermal fin application incurs additional manufacturing costs. Typically, thermal fins have effectiveness greater than 2, while high-performing fins are greater than 5. Whereas fin efficiency is increased by employing materials with high thermal conductivity, the P/A ratio should be low and low convective heat coefficient. Fin efficiency must be between 0 and 1. Most efficient fin applications are in the range of 0.9–0.95. Fin efficiency and fin effectiveness are two important design parameters in designing a thermal fin [46]. Designers should balance these parameters by investigating the most optimal design.

$$\eta\varepsilon = \frac{q\text{with fin}}{q\text{without fin}} \tag{16}$$

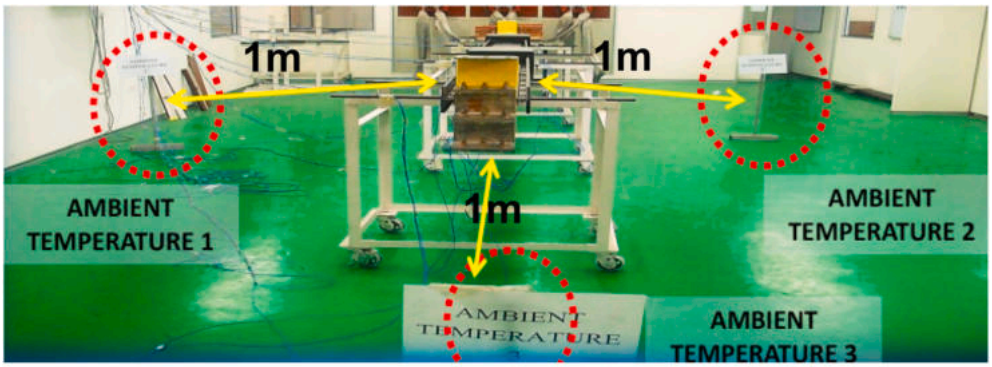

(a) Actual experimental setup

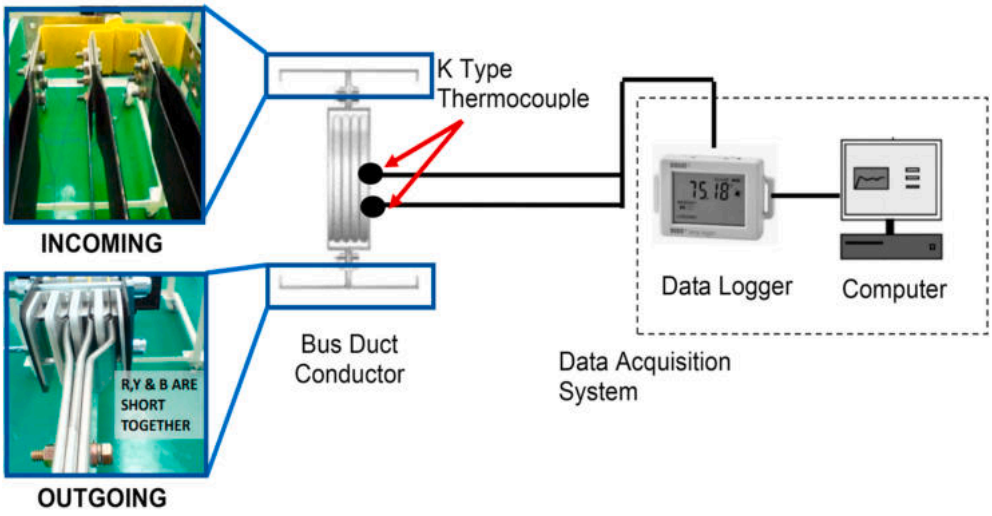

(b) Schematic diagram of the setup

Fig. 7. Setup (a) Actual experimental setup, (b) Schematic diagram of the setup.

Table 3
IEC 61439-6 temperature rise specifications.

Part Name	Temperature Rise Limit (°C)	Maximum Temperature Rise A (°C)	Max Ambient Temperature B (°C)	Total Absolute Temperature A + B (°C)
Conductor	105.0	86.0	30.0	116.0
Joint	105.0	85.8	30.0	115.8
Casing	55.0	54.8	30.0	84.8

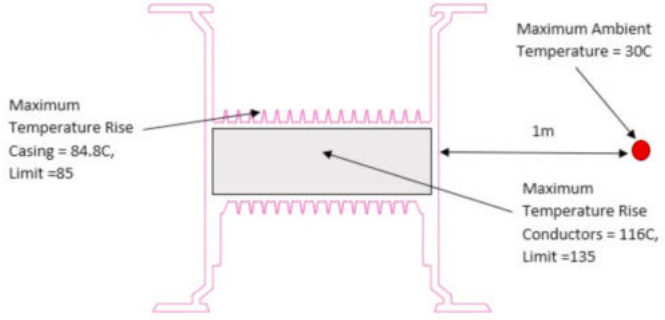

Fig. 8. Experimental results show temperature rise for different parts.

$$\eta f = \frac{q\ \text{fin}}{q\ \text{max}} \tag{17}$$

6.2. Fin effectiveness

The temperature of the bus duct housing without thermal fins was on average 92.45 °C. However, the temperature of the bus duct housing with thermal fins, as stated previously, was 81.3 °C. A significant difference in temperature of 13.7% clearly shows that the thermal fins effectively reduce the average temperature of the bus duct housing. The heat transfer rate of the bus duct housing without fins was 1.7511 W. Thus, equation (16) determined that the fin effectiveness of the original bus duct housing design is 1.055.

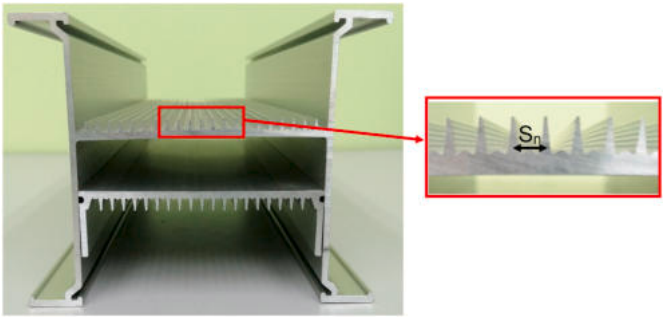

Fig. 9. Fin Pitch of bus duct conductor.

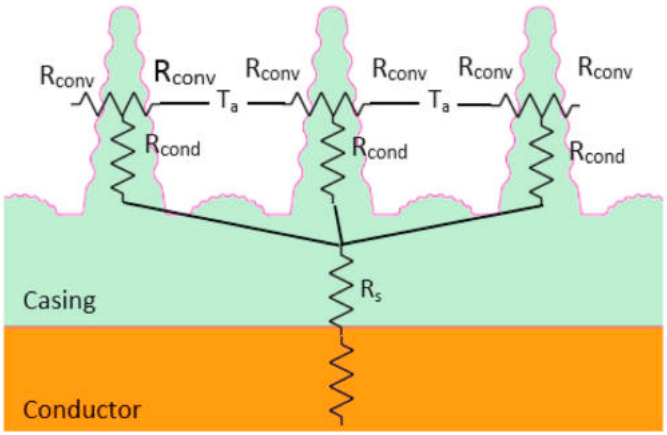

Fig. 10. Thermal resistance network diagram.

6.3. Fin efficiency

In order to investigate the fin efficiency of the thermal fins, equation (17) was employed. The thermal conductivity of the aluminum housing was set to infinite. This condition was simulated to obtain the maximum heat transfer rate from the bus duct housing. It was observed that the temperature of the entire bus duct housing remained constant without any temperature rise. The maximum total heat transfer rate was 2.28058 W. Hence, the fin efficiency of the current geometry is 0.81.

7. Results & discussion

7.1. Fin pitch (s_n) variation

In order to investigate the effect of fin pitch variation (Fig. 9), the numerical study was conducted for five fin pitch sizes, which are s_1 = 1.0 mm, s_2 = 1.5 mm, s_3 = 2.0 mm, s_4 = 3.0 mm, and s_5 = 4.0 mm. Shorter fin pitch gaps were expected to give better thermal performance than longer fin pitch sizes. The present bus duct has a fin pitch size of 2 mm. The investigated fin pitch sizes were set at decrements of 0.5 mm and increments of 1 mm from the present size (2 mm). The thermal resistance of the fin pitch used in the experiment is presented using a thermal resistance network (Fig. 10).

7.2. Effect on the thermal performance

Several physical changes were observed as the fin pitch gap increased from 1 mm to 4 mm. The total number of fins decreased from 20 to 11; consequently, the surface area exposed to the fluid decreased as well (Fig. 11). These physical changes were the primary contributor to the difference in thermal performance. The numerical analysis discovered that the average surface temperature of the bus duct's aluminium casing decreased from 354.82 K (81.67 °C) to 353.65 K (80.5 °C), as the fin pitch gap decreased from 4 mm to 1 mm, which is a 1.45% decrease in average surface temperature (Fig. 12 and Fig. 17).

In order to understand the difference in thermal performance as the fin pitch gap is decreased, an analytical approach using a thermal resistance network is employed (Fig. 10). Thermal resistance networks effectively approximate the effect of heat sources and heat transfer from that source to the surrounding domain.

The heat from the copper conductor is due to Joule heating or Ohmic heating. The heat travels outwards in all directions until it reaches the conductor boundary, where it comes into contact with the EM6 layer, which is 0.000125 mm thick. From there onwards, the heat travels through the heatsink until it reaches the heat sink's fins. The fins are extended surfaces that facilitate the dissipation of heat. This is accomplished by increasing the surface area exposed to the fluid domain. The heat dissipation path from the copper conductor to the heat sink and the surrounding environment is thwarted by thermal resistance. Hence, the thermal performance must consider both conduction and convection resistance.

Thermal resistance is often described as the quantification of how difficult it is for heat to be conducted from one point to another. It is commonly represented by the quotient of the difference in temperature by the heat flow between these 2 points (Equation (20)). The total resistance (R_{sa}) to heat transfer from the copper bus bar conductor to the ambient, as displayed in Fig. 10, can be expressed as the sum of the following resistance values, as shown in Equation (21). R_s is the conduction resistance of the aluminium casing constant among all fin pitch variations. R_f is the sum of the conduction and convection resistance through each heat sink fin (Equation (22)). Thermal resistance can be considered in the same manner as electrical resistance. Hence, the thermal resistance of each fin has to be treated as parallel to each other and can be approximated using Equations (18) and (23).

The analytical analysis observed that as the fin pitch increased, so

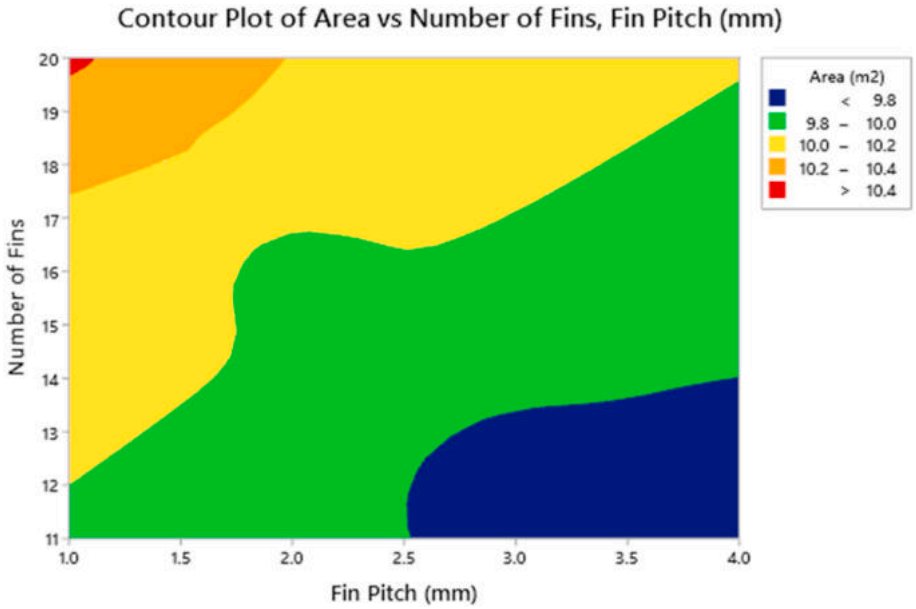

Fig. 11. Contour plot of area VS number of fins, fin pitch.

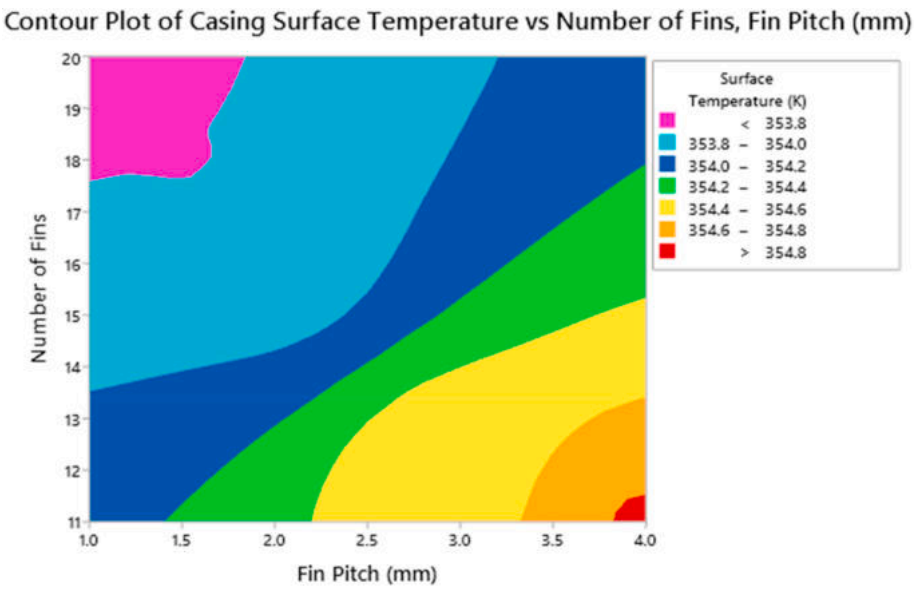

Fig. 12. Contour plot of temp VS number of fins, fin pitch.

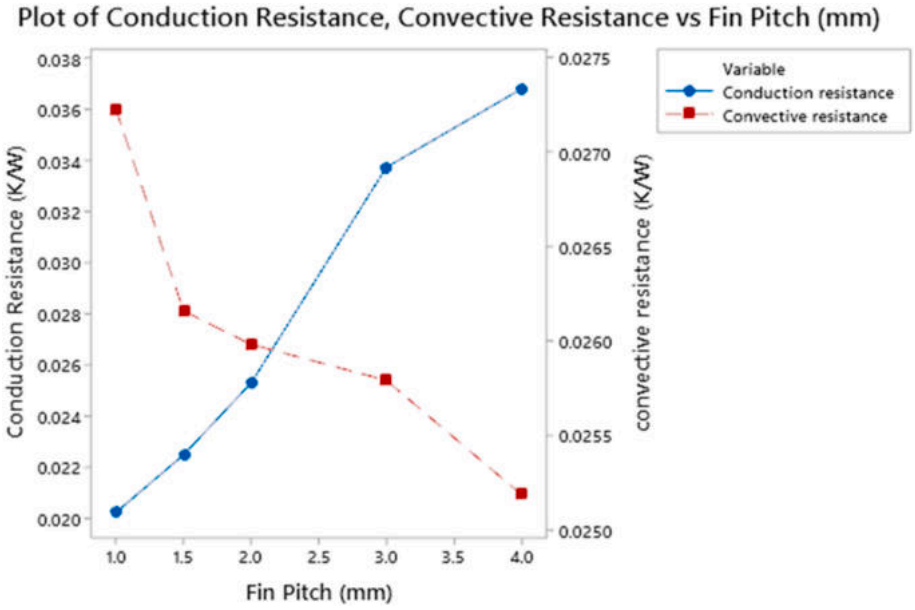

Fig. 13. Conduction & convective resistance VS fin pitch (mm).

did the conduction resistance (Fig. 13). Thus, resulting in a decrease in heat flux from the fin base to the fin tip.

$$Rd = \frac{L}{AK} \tag{18}$$

$$\varnothing q = -K\frac{\partial T(x)}{\partial x} \tag{19}$$

$$\text{Thermal resistance } R_{th} = \frac{T1 - T2}{Heat\ Flow} \tag{20}$$

$$R_{sa} = R_s + R_f \tag{21}$$

$$R_f = R_{cond} + R_{conv} \tag{22}$$

$$\frac{1}{\text{Rcond}} = \left(\frac{1}{Rd}\right) X\ No.of\ Fins \tag{23}$$

$$R_{conv} = \frac{1}{h\ X\ A} \tag{24}$$

where,

$\varnothing q$ = heat flux (W/m^2)
Rd = Thermal conduction resistance of a single fin (K/W).
h = Convective heat transfer coefficient (W/(m^2 K)).
A = Surface area exposed to fluid (m^2).
R_{sa} = Total resistance to heat transfer from heat source to ambient (K/W)
R_{conc} = Convective resistance (K/W)
R_{cond} = Conduction resistance (K/W)
K = Thermal Conductivity (W/(m·K))

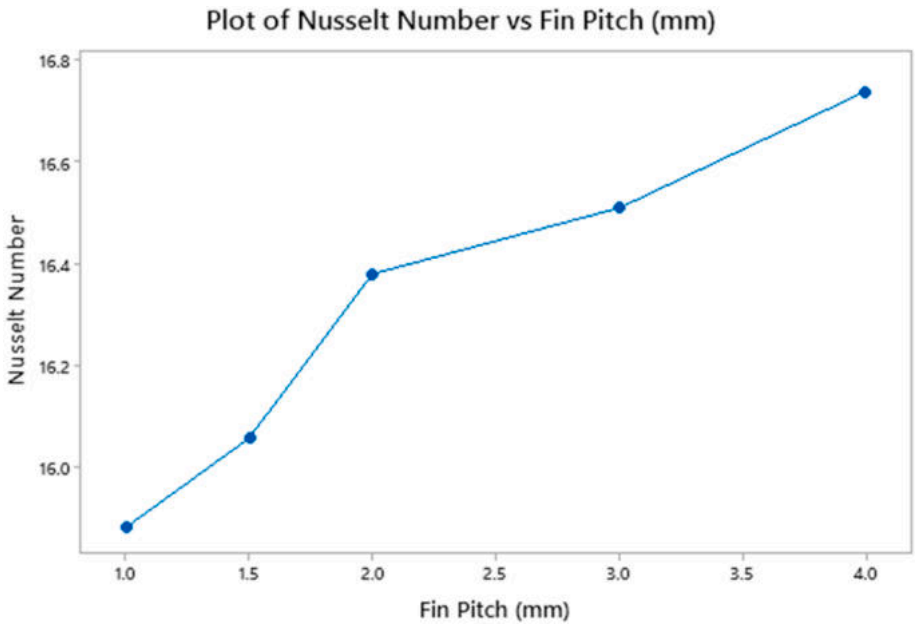

Fig. 14. Plot of Nusselt Number VS Fin Pitch of bus duct conductor.

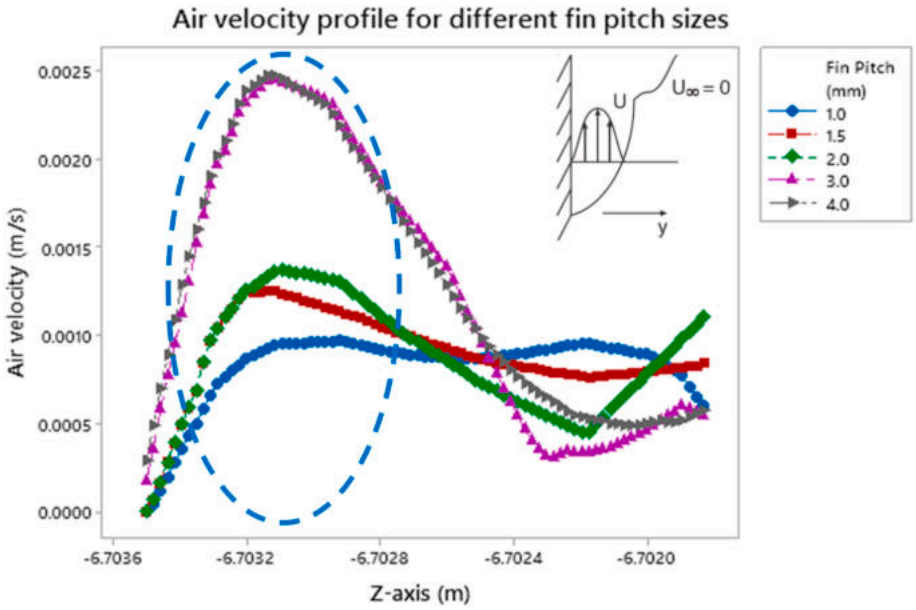

Fig. 15. Air velocity profile for different fin pitch sizes.

7.3. Effect on the fluid flow

However, the opposite is true for convection resistance. Convection plays the most crucial role in dissipating the heat from the bus bar casing. Convective heat transfer is a function of the exposed surface area to the fluid region, the temperature difference between the surface of the bus bar casing and the fluid at a bulk temperature, the fluid velocity, and heat flux.

Therefore, to assess the quality of convective heat transfer from the surface of the bus duct casing, the dimensionless number called Nusselt number was employed. Nusselt number is interpreted as the ratio of heat transfer by convection to conduction across the fluid layer of thickness L. A larger value of the Nusselt number implies enhanced heat transfer by convection. The Nusselt number for this study was between 15.88 and 16.74. The 4 mm fin pitch case yielded the highest Nusselt number of 16.74.

Longer fin pitch gaps were observed to have a higher Nusselt number than shorter fin pitch gaps (Fig. 14). This finding can be attributed to a longer fin pitch having a higher surface heat transfer coefficient (Fig. 16) and smaller convective thermal resistance (Fig. 13). Convective thermal resistance was calculated using equation (24). This finding was supported by the Nusselt number, surface heat transfer coefficient (CTE), and the fluid velocity profile analysis as plotted in Figs. 14–17. A fin pitch gap of 1 mm shows the lowest Nusselt number, surface CTE, and fin effectiveness.

The air velocity distribution adjacent to the thermal fin was also studied to better understand the hydrodynamic boundary layer on the fins surface. A fluid layer gets attached to the surface wall during the flow due to the frictional force. At a no-slip condition, the velocity of this layer is zero; with the increase in distance, the velocity of the flow

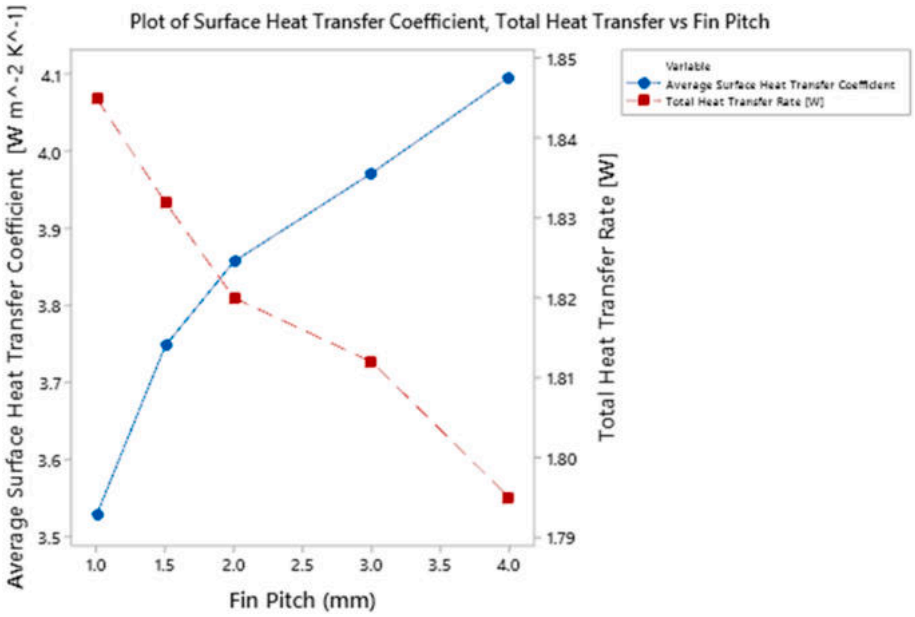

Fig. 16. The plot of Average Surface Heat Transfer Coefficient, Total Heat Transfer Rate vs. Fin Pitch Gap.

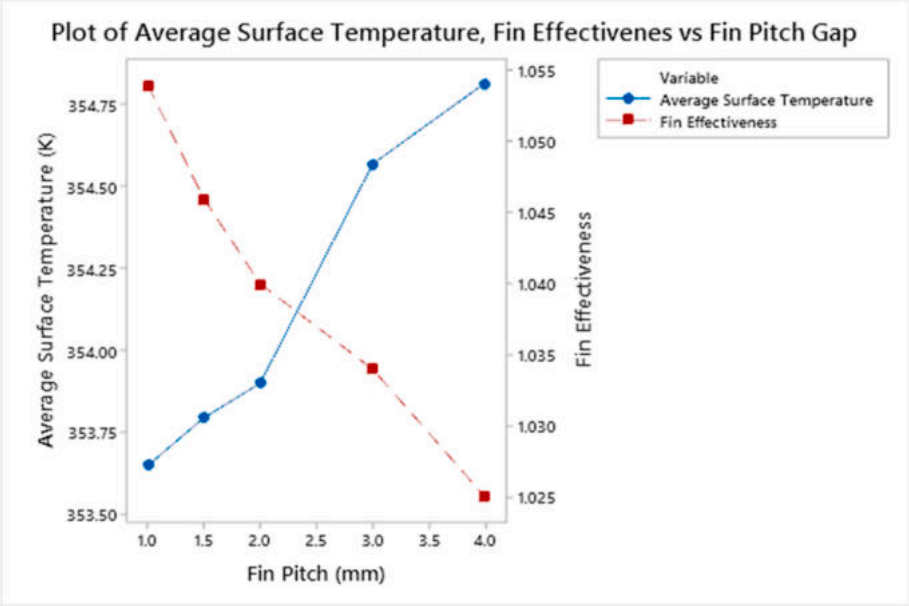

Fig. 17. The plot of average surface temperature (K), fin effectiveness vs. fin pitch gap.

increases. At a certain point, the velocity becomes one with the free-stream velocity, v. This area where the velocity transitions from zero to the free stream velocity, influenced by the shear stress in the fluid, is called the hydrodynamic boundary layer. The hydrodynamic boundary layer was studied by sampling the velocity distribution along a horizontal line between the fins (Table 4). It is evident from Fig. 15 that 4 mm and 3 mm fin pitches have the highest fluid flow velocity (0.0025 ms^{-1}), followed by fin pitches of 2 mm, 1.5 mm, and 1 mm. Higher air velocity corresponds to a higher surface heat transfer coefficient (Fig. 16). The convective coefficient depends on the thickness of the stagnant air molecules' boundary layer and the air molecules' velocity within the boundary layer. These molecules closely mimic a layer of air that acts as a blanket to insulate the fin surfaces resulting in a choking effect. Air is a poor conductor of heat. Slower air molecules result to lower heat transfer. Thus, the heat is effectively kept inside the metal, preventing effective convective heat transfer.

Table 4 depicts the velocity contour of the fluid flow regime adjacent to the heat sinks of varying fin pitch gaps. The fluid velocity contour reveals and further reaffirms that increasing the fin pitch gap size improves and enhances the fluid flow regime adjacent to the fins on the bus duct casing. As the fins become further apart, the fluid flow adjacent to the fins is more developed and faster from the fin tip to the fin base. This phenomenon indicates better heat dissipation to the surrounding fluid region. The developed flow may induce a "chimney effect" to increase the rate at which warm air is removed from the heat sink's surface and replaced with cooler air.

In this study, two modes of heat transfer were analyzed, which were conduction and convection heat transfer. The analysis shows that the conduction heat transfer decreases as the fin pitch gap increases, whereas the convection heat transfer increases. However, it should be

Table 4
Velocity contour and vector for different fin pitch sizes.

Fin Pitch (mm)	Velocity contour
1 mm	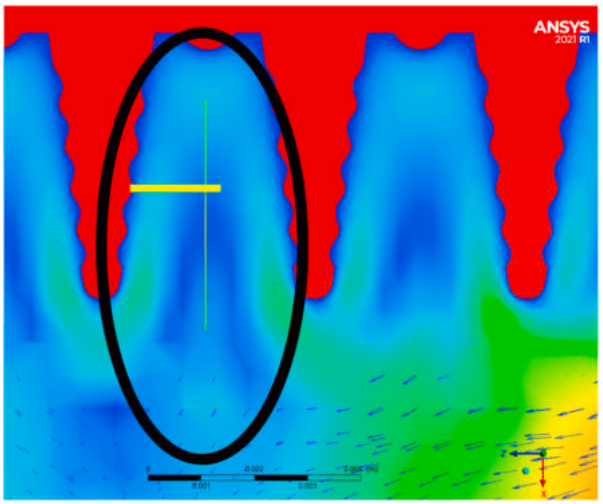
1.5 mm	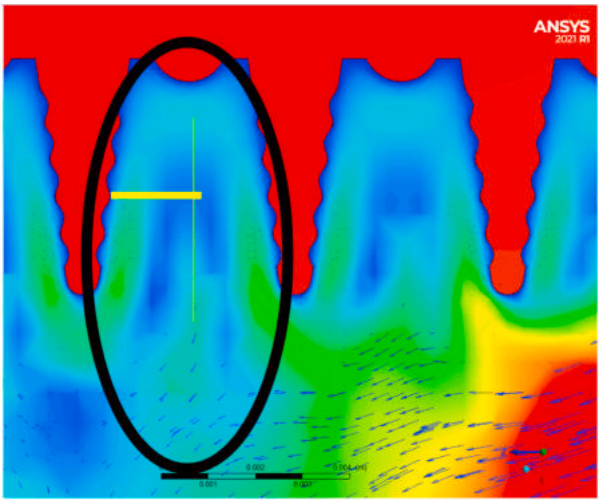
2 mm	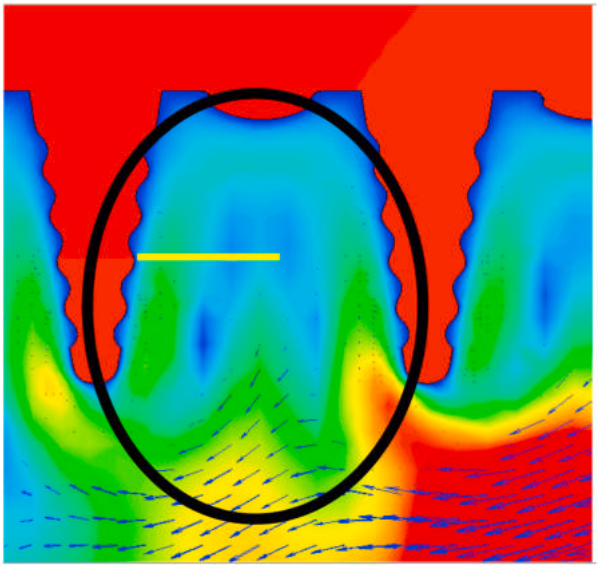

(*continued on next page*)

Table 4 (*continued*)

Fin Pitch (mm)	Velocity contour
3 mm	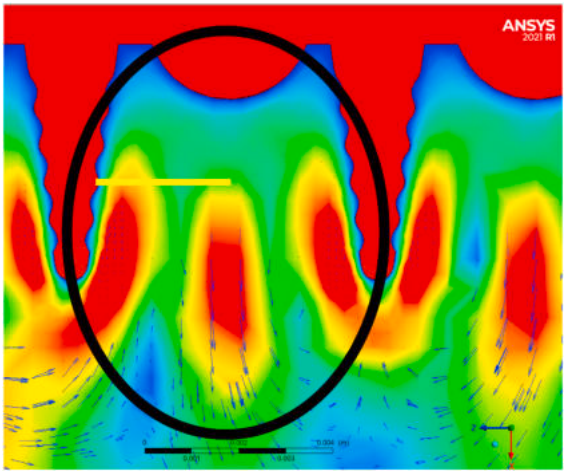
4 mm	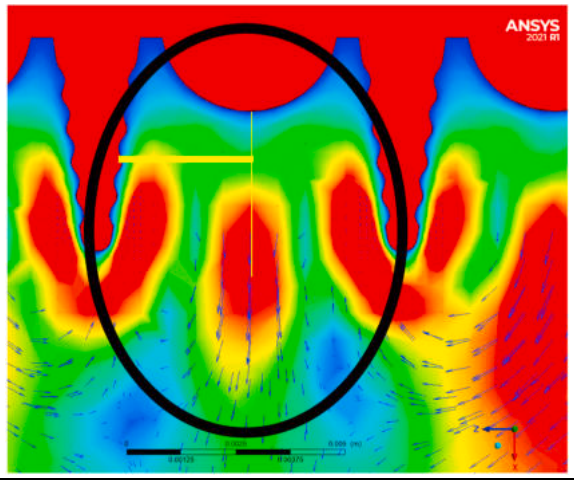

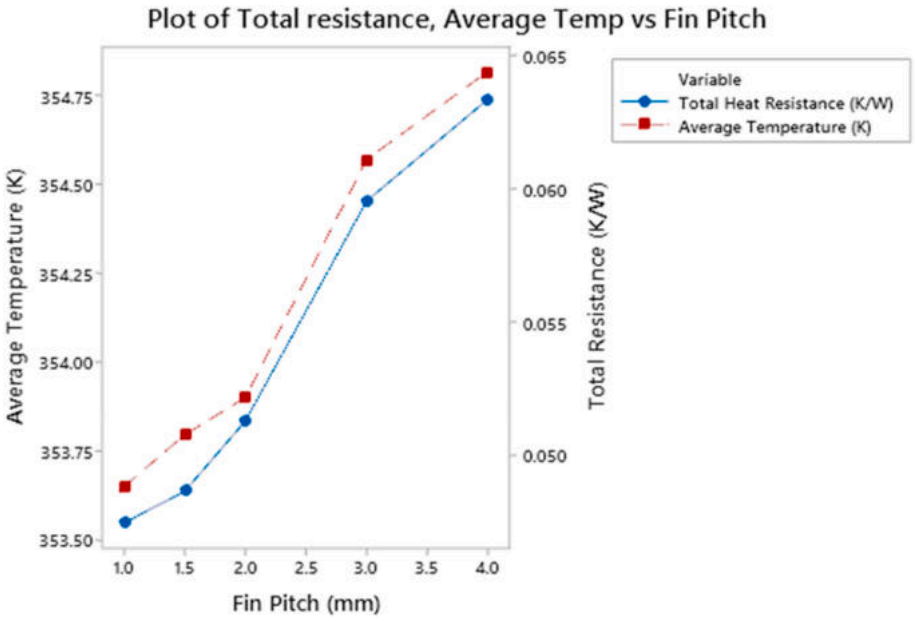

Fig. 18. Plot of Thermal Resistance, Average Temp Vs Fin Pitch of bus duct conductor.

Table 5
Thermal performance of various fin pitch gaps.

Fin Pitch (S_n)	1 mm	1.5 mm	2 mm	3 mm	4 mm
Average surface heat transfer coefficient [W m^-2 K^-1]	−3.528	−3.748	−3.857	−3.972	−4.097
Average temperature (K)	353.649	353.795	353.900	354.569	354.816
Total Heat Transfer Rate [W]	1.845	1.832	1.820	1.812	1.795
Fin effectiveness	1.054	1.046	1.106	1.034	1.025

made clear that as the fin pitch gap increases, the total resistance (Equation (22)) increases, as shown in Fig. 18. This situation increases the average surface temperature and decreases the fin effectiveness. A similar trend was also concluded by several other studies [47–50]. Table 5 summarizes the thermal performance of various fin pitch gaps.

Regression analysis was performed by setting fin pitch gap (F_p) as the regressor variable, whereas Nusselt Number (*Nu*) was the response variable. The analysis determined that the coefficient of determination was 0.99, suggesting an excellent quadratic association between fin thickness and Nusselt Number, as shown in Fig. 19. Equation (25) can be used to estimate the Nusselt Number within 1 mm–4 mm fin pitch sizes.

$$\mathrm{Nu} = 198.6 + 15.58\ \mathrm{F_p} - 1.829\ \mathrm{F_p^2} \tag{25}$$

7.4. Optimum fin pitch

Closely packed fins provide more surface area for heat transfer. However, they have a lower heat transfer coefficient (due to the extra resistance of additional fins). The heat transfer coefficient will be higher but the surface area will be smaller for a heat sink with widely spread fins. As a result, an ideal spacing maximises natural convection from the heat sink. Rohsenow and Bar-Cohen [51] provided the following recommendation (Equation (26)) for the ideal fin spacing for vertical, heat-dissipating plates under the assumption of two-dimensional flow.

$$S_{Opt} = 2.714\frac{L}{Ra^{\frac{1}{4}}} \tag{26}$$

The properties of air are evaluated at film temperature (Equation (27)).

$$T_f = \frac{(T_\infty + T_s)}{2} = 55.0^\circ C = 328.15\mathrm{K} \tag{27}$$

where,

T_f = Film temperature (K)
T_∞ = Free stream temperature (K)
T_s = Wall temperature (K)

At this temperature, k = 0.02735 W/mk, v = 1.798×10^{-5}, Pr = 0.7228 and assuming ideal gas β = 0.00305. The characteristic length is L = 0.005 m

$$Ra = \frac{g\beta(T_s - T_\infty)L^3}{\nu^2}Pr = 425.21 \tag{28}$$

The optimum fin spacing is determined using Equation (26).

$$S_{Opt} = 2.714\frac{L}{Ra^{\frac{1}{4}}} = 0.003\mathrm{m}$$

From Equation (29), the Grashof number was calculated

$$Ra = GrPr \tag{29}$$

$$Gr = 588.28$$

The simplified analytical calculation above yielded an optimum fin spacing of 0.003 m. However, the numerical analysis suggested a lower optimum fin spacing of 0.001 m instead. This deviation may arise due to the tapered fin shape of the actual geometry as compared to the analytical analysis, which assumes a vertical plate. The tapered fin shape reduces airflow resistance, thus allowing smaller fin spacing, as also reported by Anil Kumar Rao and Vandana Somkuwar [52].

8. Conclusion

In this study, the effect of fin pitch variation is investigated using the commercial CFD code, ANSYS FLUENT 2021R. Five different fin pitch sizes were considered: $s_1 = 1.0$ mm, $s_2 = 1.5$ mm, $s_3 = 2.0$ mm, $s_4 = 3.0$ mm and $s_5 = 4.0$ mm. Based on this study, the average surface temperature decreases as the fin pitch is decreased. The simulation results revealed that conduction resistance increased as the fin pitch size increased while convective resistance decreased. However, the total

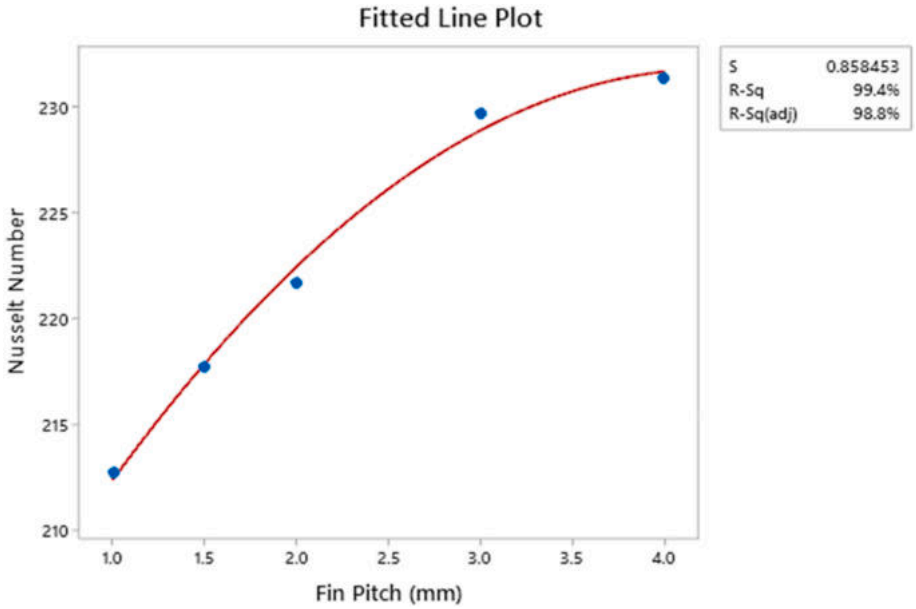

Fig. 19. Regression Model for Nusselt Number Vs Fin Pitch of bus duct conductor.

heat resistance increased. The best fin pitch size was $s_1 = 1$ mm, exhibiting superior thermal performance over the other fin pitches. The 1 mm fin pitch yielded the highest fin effectiveness (1.054) and a total heat transfer rate (1.845 W). The current findings are expected to be useful as a reference in the heat sink design and enhancement of thermal performance for the bus duct conductor.

Declaration of competing interest

The authors declare that they have no known competing financial interests or personal relationships that could have appeared to influence the work reported in this paper.

Data availability

No data was used for the research described in the article.

Acknowledgement

Acknowledgement to "Collaborative Research in Engineering, Science and Technology (CREST) grant with Project Code 304/PBAHAN/6050448/C121 and Fundamental Research Grant Scheme (FRGS) with Project Code FRGS/1/2020/TK0/USM/03/6. The authors would also like to thanks Universiti Sains Malaysia, Furutec Electrical Sdn. Bhd, and Ministry of Higher Education Malaysia for providing technical support.

References

[1] S. Thirumurugaveerakumar, M. Sakthivel, S. Valarmathi, Experimental and analytical study on the bus duct system for the prediction of temperature variations due to the fluctuation of load, J. Electr. Eng. Technol. 9 (2014) 2036–2041, https://doi.org/10.5370/JEET.2014.9.6.2036.

[2] M.A. Ismail, M.Z. Abdullah, M.A. Mujeebu, A CFD-based experimental analysis on the effect of free stream cooling on the performance of micro processor heat sinks, Int. Commun. Heat Mass Tran. 35 (2008) 771–778, https://doi.org/10.1016/j.icheatmasstransfer.2008.02.012.

[3] C.H. Huang, W.Y. Chen, A natural convection horizontal straight-fin heat sink design problem to enhance heat dissipation performance, Int. J. Therm. Sci. 176 (2022), 107540, https://doi.org/10.1016/j.ijthermalsci.2022.107540.

[4] N.P. Salunke, I.N. Wankhede, Heat transfer coefficient enhancement in natural convection from horizontal rectangular fin arrays with perforations, Int. J. Mech. Eng. Technol. (2019) 306–315.

[5] Ö. Özdilli, Design and thermal performance analysis of different type cylindrical heatsinks, Int. J. Therm. Sci. 170 (2021), https://doi.org/10.1016/j.ijthermalsci.2021.107181.

[6] H.L. Chen, C.C. Wang, Analytical analysis and experimental verification of trapezoidal fin for assessment of heat sink performance and material saving, Appl. Therm. Eng. 98 (2016) 203–212, https://doi.org/10.1016/j.applthermaleng.2015.11.131.

[7] D.S. Khudhur, R.C. Al-Zuhairy, M.S. Kassim, Thermal analysis of heat transfer with different fin geometry through straight plate-fin heat sinks, Int. J. Therm. Sci. 174 (2022), 107443, https://doi.org/10.1016/j.ijthermalsci.2021.107443.

[8] H.T. Dhaiban, M.A. Hussein, The optimal design of heat sinks: a review, J. Appl. Comput. Mech. 6 (2020) 1030–1043, https://doi.org/10.22055/jacm.2019.14852.

[9] J.H. Jang, W.M. Yan, H.C. Liu, Natural convection heat and mass transfer along a vertical wavy surface, Int. J. Heat Mass Tran. 46 (2003) 1075–1083, https://doi.org/10.1016/S0017-9310(02)00361-7.

[10] C.J. Kobus, T. Oshio, Development of a theoretical model for predicting the thermal performance characteristics of a vertical pin-fin array heat sink under combined forced and natural convection with impinging flow, Int. J. Heat Mass Tran. 48 (2005) 1053–1063, https://doi.org/10.1016/j.ijheatmasstransfer.2004.09.042.

[11] S. Liu, Y. Huang, J. Wang, International Journal of Thermal Sciences Theoretical and numerical investigation on the fi n e ff ectiveness and the fi n e ffi ciency of printed circuit heat exchanger with straight channels, Int. J. Therm. Sci. 132 (2018) 558–566, https://doi.org/10.1016/j.ijthermalsci.2018.06.029.

[12] B. Freegah, A.A. Hussain, A.H. Falih, H. Towsyfyan, CFD analysis of heat transfer enhancement in plate-fin heat sinks with fillet profile: investigation of new designs, Therm. Sci. Eng. Prog. 17 (2020), 100458, https://doi.org/10.1016/j.tsep.2019.100458.

[13] S.M. Hoi, A.L. Teh, E.H. Ooi, I.M.L. Chew, J.J. Foo, Plate-fin heat sink forced convective heat transfer augmentation with a fractal insert, Int. J. Therm. Sci. 142 (2019) 392–406, https://doi.org/10.1016/j.ijthermalsci.2019.04.035.

[14] M. Bahiraei, S. Heshmatian, Thermal performance and second law characteristics of two new microchannel heat sinks operated with hybrid nano fl uid containing graphene – silver nanoparticles, Energy Convers. Manag. 168 (2018) 357–370, https://doi.org/10.1016/j.enconman.2018.05.020.

[15] C.J. Ho, Y.C. Liu, M. Ghalambaz, W.M. Yan, Forced convection heat transfer of Nano-Encapsulated Phase Change Material (NEPCM) suspension in a mini-channel heatsink, Int. J. Heat Mass Tran. 155 (2020), https://doi.org/10.1016/j.ijheatmasstransfer.2020.119858.

[16] Y.J. Lee, S.J. Kim, Thermal optimization of the pin-fin heat sink with variable fin density cooled by natural convection, Appl. Therm. Eng. 190 (2021), 116692, https://doi.org/10.1016/j.applthermaleng.2021.116692.

[17] X. Huang, C. Shi, J. Zhou, X. Lu, G. Xu, Performance analysis and design optimization of heat pipe sink with a variable height fin array under natural convection, Appl. Therm. Eng. 159 (2019), 113939, https://doi.org/10.1016/j.applthermaleng.2019.113939.

[18] I. Tari, M. Mehrtash, Natural convection heat transfer from horizontal and slightly inclined plate-fin heat sinks, Appl. Therm. Eng. 61 (2013) 728–736, https://doi.org/10.1016/j.applthermaleng.2013.09.003.

[19] E.M. Sparrow, S.B. Vemuri, Orientation effects on natural convection/radiation heat transfer from pin-fin arrays, Int. J. Heat Mass Tran. 29 (1986) 359–368, https://doi.org/10.1016/0017-9310(86)90206-1.

[20] D. Jang, S.J. Park, S.J. Yook, K.S. Lee, The orientation effect for cylindrical heat sinks with application to LED light bulbs, Int. J. Heat Mass Tran. 71 (2014) 496–502, https://doi.org/10.1016/j.ijheatmasstransfer.2013.12.037.

[21] M. Vilarrubí, S. Riera, M. Ibañez, M. Omri, G. Laguna, L. Fréchette, J. Barrau, Experimental and numerical study of micro-pin-fin heat sinks with variable density for increased temperature uniformity, Int. J. Therm. Sci. 132 (2018) 424–434, https://doi.org/10.1016/j.ijthermalsci.2018.06.019.

[22] X. Zhang, Z. Ying, Y. Chen, X. Chen, A thermal model for calculating axial temperature distribution of overhead conductor under laboratory conditions, Elec. Power Syst. Res. 166 (2019) 223–231, https://doi.org/10.1016/j.epsr.2018.10.008.

[23] X. Dong, C. Wang, J. Liang, X. Han, F. Zhang, H. Sun, M. Wang, J. Ren, Calculation of Power Transfer Limit Considering Electro-Thermal Coupling of Overhead Transmission Line 29 (2014) 1503–1511.

[24] M. Bedkowski, J. Smolka, K. Banasiak, Z. Bulinski, A.J. Nowak, T. Tomanek, A. Wajda, Coupled numerical modelling of power loss generation in busbar system of low-voltage switchgear, Int. J. Therm. Sci. 82 (2014) 122–129, https://doi.org/10.1016/j.ijthermalsci.2014.04.001.

[25] Y.K. Prajapati, Influence of fin height on heat transfer and fluid flow characteristics of rectangular microchannel heat sink, Int. J. Heat Mass Tran. 137 (2019) 1041–1052, https://doi.org/10.1016/j.ijheatmasstransfer.2019.04.012.

[26] P. Bhandari, Y.K. Prajapati, Thermal performance of open microchannel heat sink with variable pin fin height, Int. J. Therm. Sci. 159 (2021), 106609, https://doi.org/10.1016/j.ijthermalsci.2020.106609.

[27] W.H. Aldoori, The effect of fin height on forced convection heat transfer from rectangular fin array, Mater. Today Proc. (2021), https://doi.org/10.1016/j.matpr.2021.07.191.

[28] A. Bejan, S. Lorente, The constructal law of design and evolution in nature, Philos. Trans. R. Soc. B Biol. Sci. 365 (2010) 1335–1347, https://doi.org/10.1098/rstb.2009.0302.

[29] H. Feng, Z. Zhang, L. Chen, Y. Ge, J. Yu, Constructal design for tree-shaped compound heat transfer channel in a disc heat generation body, Int. Commun. Heat Mass Tran. 132 (2022), 105929, https://doi.org/10.1016/j.icheatmasstransfer.2022.105929.

[30] K. Sun, H. Feng, L. Chen, Y. Ge, Constructal design of a cooling channel with semi-circular sidewall ribs in a rectangular heat generation body, Int. Commun. Heat Mass Tran. 134 (2022), 106040, https://doi.org/10.1016/j.icheatmasstransfer.2022.106040.

[31] Z. Zhang, H. Feng, L. Chen, Y. Ge, Multi-objective constructal design for compound heat dissipation channels in a three-dimensional trapezoidal heat generation body, Int. Commun. Heat Mass Tran. 127 (2021), 105584, https://doi.org/10.1016/j.icheatmasstransfer.2021.105584.

[32] H. Feng, L. Chen, Z. Wu, Z. Xie, Constructal design of a shell-and-tube heat exchanger for organic fluid evaporation process, Int. J. Heat Mass Tran. 131 (2019) 750–756, https://doi.org/10.1016/j.ijheatmasstransfer.2018.11.105.

[33] H. Feng, L. Chen, S. Xia, Constructal design for disc-shaped heat exchanger with maximum thermal efficiency, Int. J. Heat Mass Tran. 130 (2019) 740–746, https://doi.org/10.1016/j.ijheatmasstransfer.2018.11.003.

[34] H. Feng, C. Cai, L. Chen, Z. Wu, G. Lorenzini, Constructal design of a shell-and-tube condenser with ammonia-water working fluid, Int. Commun. Heat Mass Tran. 118 (2020), 104867, https://doi.org/10.1016/j.icheatmasstransfer.2020.104867.

[35] H. Feng, L. Chen, W. Tang, Y. Ge, Optimal Design of a Dual-Pressure Steam Turbine for Rankine Cycle Based on Constructal Theory, 2022, pp. 1–22.

[36] H. Feng, Z. Xie, L. Chen, Z. Wu, S. Xia, Constructal design for supercharged boiler superheater, Energy 191 (2020), 116484, https://doi.org/10.1016/j.energy.2019.116484.

[37] H. Feng, W. Tang, L. Chen, J. Shi, Z. Wu, Multi-objective constructal optimization for marine condensers, Energies 14 (2021) 1–19, https://doi.org/10.3390/en14175545.

[38] E. Rahmani, T. Moradi, A. Fattahi, M. Delpisheh, N. Karimi, F. Ommi, Z. Saboohi, Numerical simulation of a solar air heater equipped with wavy and raccoon-shaped fins: the effect of fins' height, Sustain. Energy Technol. Assessments 45 (2021), 101227, https://doi.org/10.1016/j.seta.2021.101227.

[39] A.A. Sertkaya, M. Ozdemir, E. Canli, Effects of pin fin height, spacing and orientation to natural convection heat transfer for inline pin fin and plate heat sinks by experimental investigation, Int. J. Heat Mass Tran. 177 (2021), 121527, https://doi.org/10.1016/j.ijheatmasstransfer.2021.121527.

[40] Y.T. Yang, H. Sen Peng, Numerical study of pin-fin heat sink with un-uniform fin height design, Int. J. Heat Mass Tran. 51 (2008) 4788–4796, https://doi.org/10.1016/j.ijheatmasstransfer.2008.02.017.
[41] Y. Cormier, P. Dupuis, A. Farjam, A. Corbeil, B. Jodoin, Additive manufacturing of pyramidal pin fins: height and fin density effects under forced convection, Int. J. Heat Mass Tran. 75 (2014) 235–244, https://doi.org/10.1016/j.ijheatmasstransfer.2014.03.053.
[42] M.S. Abdul Aziz, M.Z. Abdullah, C.Y. Khor, A. Jalar, F. Che Ani, CFD modeling of pin shape effects on capillary flow during wave soldering, Int. J. Heat Mass Tran. 72 (2014) 400–410, https://doi.org/10.1016/j.ijheatmasstransfer.2014.01.037.
[43] M.S.A. Aziz, M.Z. Abdullah, C.Y. Khor, F.C. Ani, Influence of pin offset in PCB through-hole during wave soldering process: CFD modeling approach, Int. Commun. Heat Mass Tran. 48 (2013) 116–123, https://doi.org/10.1016/j.icheatmasstransfer.2013.08.003.
[44] M.S. Abdul Aziz, M.Z. Abdullah, C.Y. Khor, A. Jalar, F. Che Ani, N. Yan, C. Cheok, Finite volume-based simulation of the wave soldering process: influence of the conveyor angle on pin-through-hole capillary flow, Numer. Heat Tran. 69 (2016) 295–310, https://doi.org/10.1080/10407782.2015.1069675.
[45] D.S. Khudhur, R.C. Al-Zuhairy, M.S. Kassim, Thermal analysis of heat transfer with different fin geometry through straight plate-fin heat sinks, Int. J. Therm. Sci. 174 (2022), 107443, https://doi.org/10.1016/j.ijthermalsci.2021.107443.
[46] J.-C. Han, Analytical Heat Transfer, 2016, https://doi.org/10.1201/b12870.
[47] H.H. Wu, Y.Y. Hsiao, H.S. Huang, P.H. Tang, S.L. Chen, A practical plate-fin heat sink model, Appl. Therm. Eng. 31 (2011) 984–992, https://doi.org/10.1016/j.applthermaleng.2010.10.014.
[48] P. Pongsoi, S. Pikulkajorn, S. Wongwises, Effect of fin pitches on the optimum heat transfer performance of crimped spiral fin-and-tube heat exchangers, Int. J. Heat Mass Tran. 55 (2012) 6555–6566, https://doi.org/10.1016/j.ijheatmasstransfer.2012.06.061.
[49] A.J. Jubear, EXPERIMENTAL STUDY FOR OPTIMUM FIN SPACING OF RECTANGULAR FIN ARRANGEMENTS UNDER THE INFLUENCES OF FREE CONVECTION, 2021.
[50] H. Hom, H. Kong, Heat-Exchanger performance : influence of gap width between consecutive vertical rectangular, Fin-Arrays 56 (1997) 1–8.
[51] R. Bar-Cohen, Thermally optimum spacing of ¥ ertical 3 natural gonwection cooled, Parallel Plates 106 (2018) 2–9, https://doi.org/10.1115/1.3246622.
[52] A.K. Rao, V. Somkuwar, Heat transfer of a tapered fin heat sink under natural convection, Mater. Today Proc. 46 (2021) 7886–7891, https://doi.org/10.1016/j.matpr.2021.02.565.